

Topological insulators and metals in atomic optical lattices

Tudor D. Stanescu,¹ Victor Galitski,¹ J. Y. Vaishnav,² Charles W. Clark,² and S. Das Sarma¹

¹*Department of Physics, Joint Quantum Institute and Condensed Matter Theory Center, University of Maryland, College Park, Maryland 20742-4111, USA*

²*Joint Quantum Institute, National Institute of Standards and Technology, Gaithersburg, Maryland 20899, USA*
(Received 27 January 2009; revised manuscript received 24 March 2009; published 28 May 2009)

We propose the realization of topological quantum states in a cold-atom system, using a two-dimensional hexagonal optical lattice and a light-induced periodic vector potential. A necessary condition for observing the topological states is the realization of a confining potential with a flat bottom and sharp boundaries. To probe the topological states, we propose to load bosons into the characteristic edge states and image them directly. The possibility of mapping out the edge states and controlling the optical lattice and vector potentials offers opportunities for exploring topological phases with no equivalent in condensed-matter systems.

DOI: [10.1103/PhysRevA.79.053639](https://doi.org/10.1103/PhysRevA.79.053639)

PACS number(s): 03.75.Lm, 67.85.-d, 03.65.Vf, 73.43.-f

I. INTRODUCTION

Cold-atom systems offer a platform for implementing quantum dynamics that provides flexible conditions of observation and control. An emerging theme in this field, which has been investigated theoretically but is just beginning to receive experimental attention, is the construction of synthetic Abelian and non-Abelian gauge potentials coupled to neutral atoms. In this paper, we propose a cold-atom realization of a topological insulator using a light-induced periodic vector potential. More importantly, we establish the necessary conditions for the realization of topological states in confined systems and we identify a powerful tool for probing these states by mapping out the characteristic edge states using bosons.

A solid-state insulator can be defined as a system with purely local electronic properties [1]. The existence of a bulk gap is insufficient to ensure the locality of all electronic properties. Certain strongly correlated systems, such as the fractional quantum Hall fluids, offer examples of phases having bulk gaps, yet being topologically distinct [2]. Such topological insulators can exist even in the absence of interactions; typical examples are the integer quantum Hall fluids or the quantum spin Hall states [3–5] and their three-dimensional generalizations [6]. One defining characteristic of these systems is the existence of chiral gapless edge or surface states robust to disorder effects and interactions. Such edge or surface states were recently observed experimentally in several solid-state systems [7,8]. The basic features of these states are intrinsically linked to the topological properties of the system, but their detailed structure is dictated by the boundary. Controlling the boundary is a rather difficult task in solid-state systems but could be achieved with ultracold atoms.

A great advantage of the optical lattices is that various terms in the Hamiltonian can be explicitly controlled experimentally, which in contrast to solid-state systems allows for tuning the properties of the edge states. The realization of a topological insulator with cold atoms opens a series of very exciting prospects: (i) the possibility of direct real-space imaging of the edge states [9], (ii) the possibility of testing the stability of the chiral edge modes in the presence of weak

disorder and interactions, and (iii) the possibility of studying transitions between a topological insulator and other phases. The main challenges in building a topological insulator with cold atoms are (i) generating the vector potential, (ii) controlling the trap potential and manipulating the boundaries, and (iii) measuring a topological insulating state, i.e., imaging the edge states. In this paper, we address explicitly the last two problems within a realization of the Haldane model using ultracold atoms. The ingredients necessary for this realization and the theoretical method used to describe the resulting cold-atom system are presented in Sec. II. The conditions for the trap potential consistent with the existence of topological edge states are established in Sec. III, together with a proposal for observing these states experimentally.

II. HALDANE MODEL IN ATOMIC OPTICAL LATTICES

We study the stability of topological quantum states in the presence of confining potentials within a realization of the Haldane model [4] using cold atoms in an optical lattice [10]. We propose a method for identifying and characterizing topological quantum states by mapping out the characteristic edge states using bosons. The Haldane model consists of a tight-binding representation of motion on a hexagonal lattice with direction-dependent complex next-nearest-neighbor hoppings as the key feature. The imaginary components of the hopping matrix elements are determined by an effective vector potential $\mathbf{A}(\mathbf{r})$ that generates a periodic “magnetic” field with zero total flux through the unit cell. We propose the use of a light-induced gauge potential that can be realized in a system of multilevel atoms interacting with a spatially modulated laser field [10–19]. Within these schemes, the multilevel atoms interact with laser beams characterized by spatially varying Rabi frequencies and experience an effective pseudo-spin-dependent gauge potential. Since our proposal does not require spin-dependent gauge potentials, one may even be able to utilize a simpler scheme [20]. The hexagonal lattice potential is given by the superposition of three coplanar standing waves characterized by the wave vectors $\mathbf{k}_1 = (0, \frac{2\pi}{3a})$, $\mathbf{k}_2 = (\frac{\pi}{\sqrt{3}a}, \frac{\pi}{3a})$, and $\mathbf{k}_3 = (-\frac{\pi}{\sqrt{3}a}, \frac{\pi}{3a})$, respectively. The minima of this potential generate a hexagonal lattice

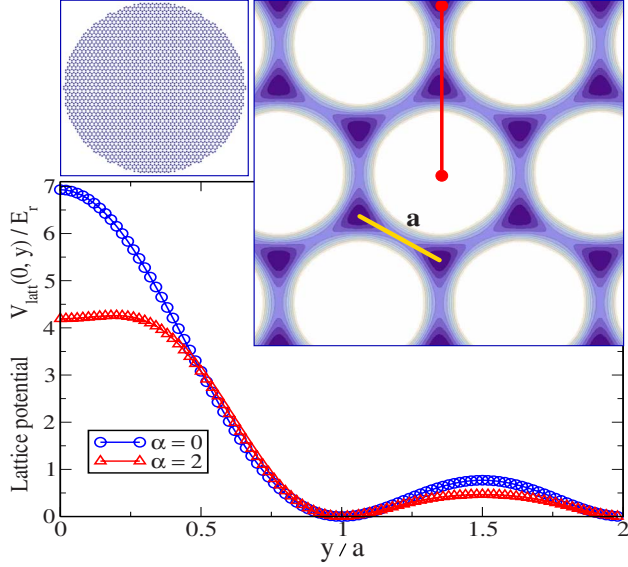


FIG. 1. (Color online) Optical lattice potential formed by the superposition of three standing waves (see main text) and generating a two-dimensional hexagonal lattice with lattice constant a . The effective confining potential along the segment $(0,0) - (0,2a)$ [vertical red (dark gray) line in the upper right panel] is shown in the absence of a vector potential (blue circles) and for $\mathbf{A} \neq 0$ (red triangles). Inset: typical cluster used in the calculations consisting of a disk-shaped piece of hexagonal lattice with radius $R \approx 39a$.

with lattice constant a . The resulting single-particle Hamiltonian is

$$H = \frac{1}{2m} [\mathbf{p} - \mathbf{A}(\mathbf{r})]^2 + V_0 \sum_{i=1}^3 \cos^2(\mathbf{k}_i \cdot \mathbf{r}) + V_c(\mathbf{r}). \quad (1)$$

Here m is the particle mass; \mathbf{p} is the momentum; $\mathbf{A} = (\alpha \mathcal{A}_x, 0)$ is the vector potential, where $\mathcal{A}_x(\mathbf{r}) = \sin(\frac{4\pi y}{3})$, and α is the strength of the gauge potential; V_0 defines the depth of the optical lattice; and V_c describes an additional confinement that will be discussed in detail below. The term $\mathbf{A}^2/2m$ from Eq. (1) represents a contribution to the lattice potential that does not have hexagonal symmetry and, therefore, will distort the lattice. This distortion does not affect the nature and the basic properties of the topological insulator if α does not exceed a certain critical value but has quantitative implications for the band structure. For simplicity, we use in our calculations the symmetric vector potential $\mathcal{A}(\mathbf{r}) = [\sin(4\pi y/3) + \cos(2\pi x/\sqrt{3})\sin(2\pi y/3), -\sqrt{3}\sin(2\pi x/\sqrt{3})\cos(2\pi y/3)]$. The total optical lattice potential, including the $\mathbf{A}^2/2m$ term coming from the symmetric vector potential, is shown in Fig. 1.

We solve the quantum problem associated with Hamiltonian (1) within a simple tight-binding approximation. We use the recoil energy $E_r = \frac{(\pi/a)^2}{2m}$ as energy unit and the lattice constant a as length unit. The total effective lattice potential V_{lat} , which includes the term $\mathbf{A}^2/2m$, has minima at the nodes of a hexagonal lattice (see Fig. 1) and takes near these minima the form $V_{\text{lat}} \approx m\omega_0^2/2(\delta x^2 + \delta y^2)$. This suggests the use of the s -wave orbitals $\phi_0^{(i)}(\mathbf{r}) = \sqrt{2}/(\pi c) \exp[-(\mathbf{r} - \mathbf{r}_i)^2/c]$ as a possible simple basis

for the tight-binding approximation. Here \mathbf{r}_i represents the position of a lattice site, $c = (4E_r)/(\pi^2\omega_0)a^2$, and we have $V_0 = 12E_r/\pi^4(a^4/c^2 - \pi^2\alpha^2a^2/4)$. The approximation holds as long as the s band is well separated from the p bands, which is the case for $c < 0.25$. However, because the second-neighbor hopping is crucial for generating the topological states [4], a small value of c will make this effect practically unobservable. In this study we choose $c = 0.2$, for which the single-band tight-binding approximation holds. However, the optimal regime for the experimental realization of the topological insulator corresponds to shallower optical lattices ($c \sim 0.3 \div 0.35$), which maximize the anomalous second-neighbor hopping and thus the insulating gap. Note that, for $E_r \sim 10$ kHz, typical values of the gap for $c = 0.2$ are in the range of several nK, so that the temperatures necessary for observing the topological insulator would be much lower than those currently accessible. The gap values increase substantially in shallow optical lattices, but detailed calculations beyond the tight-binding approximation are necessary for quantitative estimates. Note that this low-temperature limitation stems from the fact that the topological properties of the Haldane model are controlled by an anomalous second-order hopping, which in general is rather small. The other independent parameter in our calculations is α , which takes the values $\alpha = 0$ (zero vector potential) or $\alpha = 2$. The hopping parameters for the effective tight-binding model are given by $t_{ij} = \langle \phi_0^{(i)} | H | \phi_0^{(j)} \rangle$. The key contributions coming from the vector potential $\langle \phi_0^{(i)} | \mathbf{p} \cdot \mathbf{A} | \phi_0^{(j)} \rangle$ vanish if i and j are nearest neighbors and are nonzero for second-order neighbors.

Because the s -wave orbitals are not orthogonal, we also determine their overlap matrix elements $\langle \phi_0^{(i)} | \phi_0^{(j)} \rangle$. The resulting tight-binding problem is solved numerically for clusters containing up to 3696 sites (see Fig. 1).

III. CHIRAL EDGE STATES IN TOPOLOGICAL COLD-ATOM SYSTEMS

First, we consider a disk-shaped cluster with hard-wall boundary conditions $V_c(r) = \infty$ if $r > R$ and $V_c(r) = 0$ if $r < R$. The density of states (DOS) for this system is shown in Fig. 2 (panels 2 and 3). In the absence of a vector potential ($\alpha = 0$, panel 3), this quantity is similar to the graphene DOS. In the presence of a vector potential with $\alpha = 2$ (panel 2), a finite-size gap opens in the density of states.

However, the DOS in the “gap” is not exactly zero. To determine the nature of the residual in-gap states, we calculate the orbital momentum of each single-particle state $\psi_n(\mathbf{r})$ and the relative contribution γ_n to the norm $\langle \psi_n | \psi_n \rangle$ coming from a narrow ring $37a \leq r \leq 39a$ positioned at the edge of the system. This contribution vanishes for bulklike states and is on the order 1 for edge states, i.e., it represents a measure of the edgelike character of a given state. The corresponding spectrum is shown in Fig. 2. The coordinates of each dot represent the orbital momentum (x axis) and the energy (y axis) of a particular state. The edge vs bulk character of the state, as quantified by the parameter γ_n , is revealed by the color code: blue for edge states and red for bulk states. The spectrum is characterized by a gap for the bulk (red) states. Within this gap, there is a chiral edge mode (blue states). The

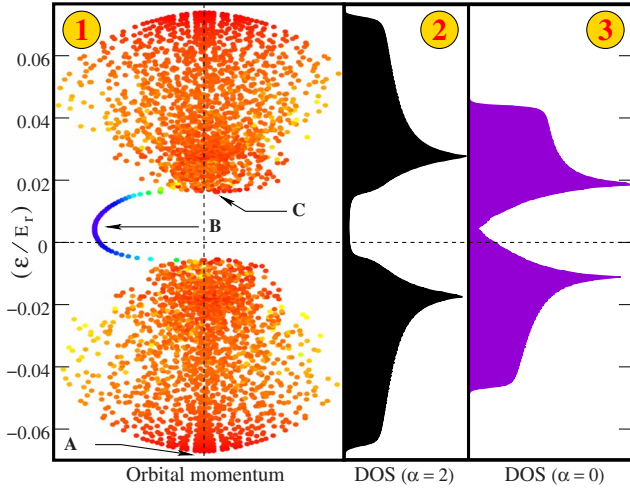


FIG. 2. (Color online) Spectrum for a cluster with a hard-wall boundary in the presence of a periodic vector potential with $\alpha=2$ (panel 1). The coordinates of each dot represent the orbital momentum in some arbitrary units (horizontal axis) and the energy ϵ (vertical axis) of a particular state. The “edge” vs “bulk” character of each state is shown by the color code, which represents the relative boundary contribution to the norm γ_n (see main text). γ_n ranges from 1 for edge states (blue: the edge mode containing state B) to 0 for purely bulk states (red: the “butterfly wings” corresponding to the upper and lower bands). Notice the chiral nature of the edge mode that populates the gap, which is responsible for the well-defined sign of the edge state orbital momentum. The DOS corresponding to this spectrum is shown in panel 2. For comparison, in panel 3 we show the DOS in the absence of a gauge potential.

chirality of the edge mode, i.e., the sign of its orbital momentum, is determined by the sign of α . To have a spatial characterization of the single-particle quantum states, we show in Fig. 3 the contour plots of $\rho_n(\mathbf{r})=|\psi_n(\mathbf{r})|^2$ for several states marked in Fig. 2: (A) the ground state, (B) a typical edge state, and (C) the lowest-energy bulk state from the upper band. Each function $\rho_n(\mathbf{r})$ is the product of a common factor $[\sum_i \phi_0^2(\mathbf{r}-\mathbf{r}_i)]^2$ associated with the underlying lattice structure and a specific envelope function (left panels in Fig. 3).

Next, we address the key question concerning the role of the confining potential V_c and the dependence of the spectrum on the boundary conditions. We replace the hard-wall boundary by (a) a quartic wall, (b) a linear step potential, and (c) a harmonic potential plus a hard wall (see top panel in Fig. 4). The corresponding expressions of the confining potential are $V_c^a(r)=\lambda_c^a(r-R_0)^4$ if $r>R_0$ (and 0 otherwise), $V_c^b(r)=\min[\lambda_c^b(r-R_1)/(R_2-R_1), \lambda_c^b]$ if $r>R_1$ (and 0 otherwise), and $V_c^c(r)=\lambda_c^c r^2$ if $r<R_2$ (and ∞ otherwise), respectively. To define a characteristic length scale associated with the confining potential, we introduce the radii R_Δ , such that $V_c(R_\Delta)=\Delta_\alpha$ and R_W , with the property $V_c(R_W)=W$. Here Δ_α is the bulk gap and W is the sum of the bandwidths of the lower and upper bands for a system with hard walls. The relevant length scale for a soft boundary produced by the confining potential V_c is given by $d_c=R_W-R_\Delta$. Our numerical calculations show that a topological insulator can be realized provided $d_c \sim a$, i.e., the boundary has a characteristic

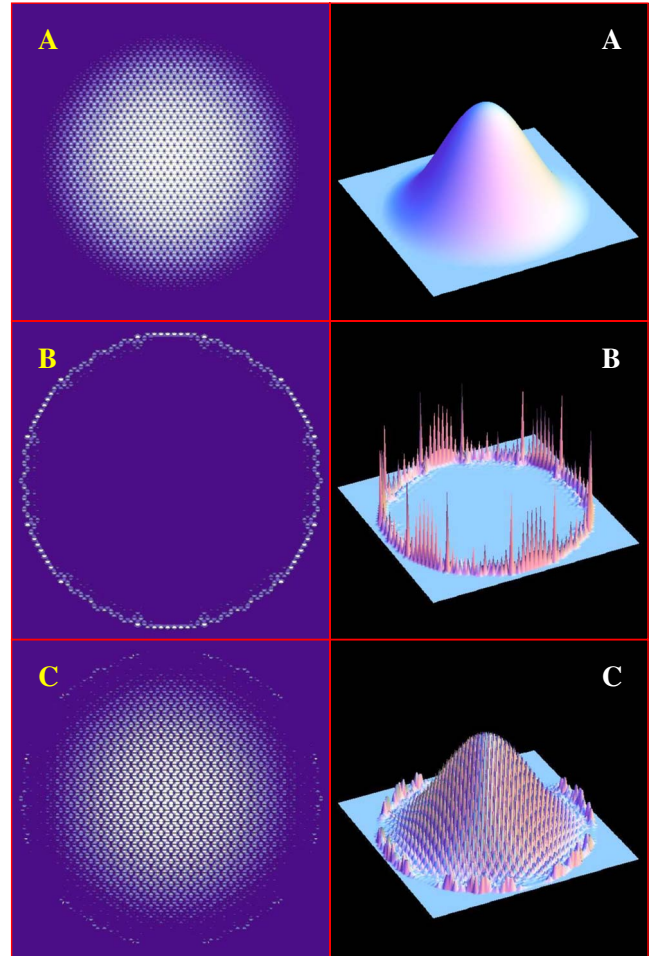


FIG. 3. (Color online) Left panels: contour plots of $\rho_n(\mathbf{r})=|\psi_n(\mathbf{r})|^2$ for the states marked in Fig. 2. The quantity $\rho_n(\mathbf{r})$ is the product between a common factor associated with the underlying hexagonal lattice structure and a state-dependent envelope function. The corresponding envelope functions are shown in the right panels. (a) represents the ground state, (b) is a typical edge state, and (c) is the lowest-energy bulk state from the upper band. The weak edge contributions in (c) are due to finite-size effects and vanish in the large cluster limit.

length on the order of the lattice constant. For example, cases (a) and (b) in Fig. 5 correspond to $R_\Delta \approx 32.5a$ and $d_c \approx 3.5a$, and in both cases the gap for bulk states is preserved. However, in contrast with the hard-wall case characterized by a featureless residual in-gap DOS (see panel 2 in Fig. 2), a system with soft boundaries has a nontrivial structure of the residual DOS (middle panels in Fig. 4). This structure emerges from two causes: (1) the orbital momentum of the chiral edge mode acquires a more complicated energy dependence and (2) additional edge states that do not belong to the chiral edge mode develop inside the gap. Both these points are illustrated in Fig. 5. The *B*-type edge states are Tamm-type states, which are formed due to the rapid variation in the confining potential and are not related to the topological properties of the insulator. The proliferation of this type of states will eventually destroy the topological quantum state for a soft enough confining potential. Finally, in the presence of a confining potential with a smoothly

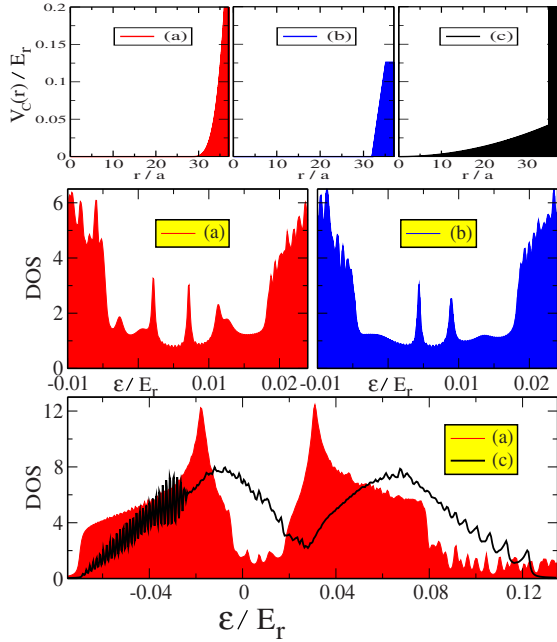


FIG. 4. (Color online) Soft boundary confining potentials (top panels): (a) quartic wall, (b) linear step, and (c) harmonic trap plus infinite wall. The turquoise (gray, $V_c < 0.025$) region corresponds to energies smaller than the gap Δ_α , while in the yellow (light gray, $V_c < 0.125$) region the energy is smaller than the bandwidth W . A confining potential with characteristic length d_c on the order of lattice spacing [(a) and (b)] preserves the bulk gap (topological insulator). The in-gap features appearing in the density of states (middle panels) are all due to edge states (see also Fig. 5). In a smoothly varying confining potential [case (c)], the bulk gap collapses for $V_c(r) > \Delta_\alpha$ (metal, see lower panel). In cases (a) and (b), the lower band is unaffected by the details of the confining potential, while the in-gap structures (middle panels) are similar. The rapid oscillations at low energies in case (c) indicate the formation of harmonic-oscillator levels.

varying component [case (c) in Fig. 4], the bulk gap collapses for $V_c(r) > \Delta_\alpha$ and the system becomes an inhomogeneous metal. Note that in the presence of the periodic vector potential $\mathbf{A}(\mathbf{r})$, the system still has chiral edge states even in the metallic phase; but they are continuously connected with the bulk states. This situation is similar to the existence of surface states in doped semiconductors [21] in the presence of the spin-orbit coupling. We conclude that in order to realize a topological insulator with cold atoms, one needs to produce a sharp boundary ($d_c \sim a$) and to minimize any smoothly varying component of the confining potential [$V_c(r) < \Delta_\alpha$].

Probing a topological state is a difficult task in atomic systems. One proposal is to perform density profile measurements on fermionic atomic systems [10,22]. Alternatively, since the nontrivial topological properties of a system are a feature of the single-particle Hamiltonian revealed by the presence of chiral edge states, we propose the direct observation of these edge states in cold-atomic systems, something one cannot easily realize in the condensed-matter context. This involves two steps: (1) loading bosons into the edge states and (2) imaging the atoms. Initially, the optical

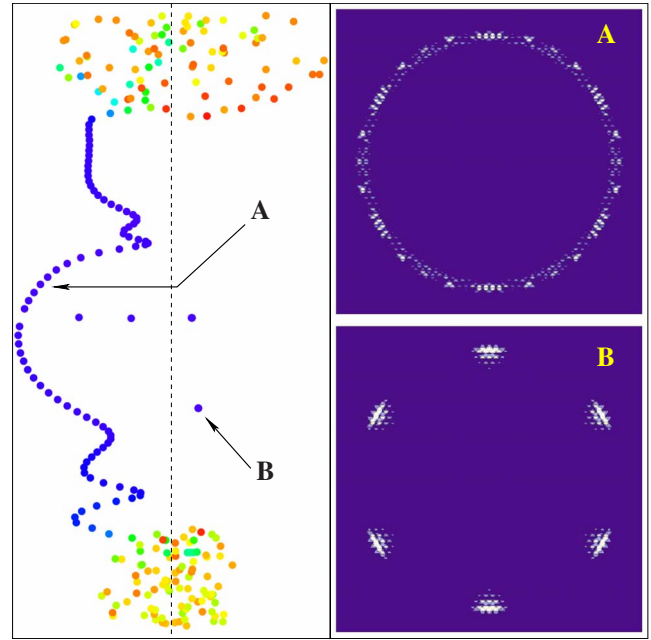


FIG. 5. (Color online) In-gap states for a system with soft boundary (quartic wall). Color code is the same as in Fig. 2. Note that all the in-gap states have edgeline character. In addition to the typical chiral edge states (a), notice the presence of Tamm-type edge states (b). These states can mix. For softer boundaries, proliferation of and mixing with the Tamm states will eventually destroy the topological insulating phase.

lattice is loaded with atoms and cooled so that the bosons occupy only the lowest-energy single-particle states. Such states have small spatial overlap with the chiral states, so direct excitation of the bosons into chiral states will be difficult. However, it is possible to use a sequence of staged resonance excitation processes to promote atoms into states of increasing angular momentum, for example, via a sequence of the two-photon-stimulated Raman transitions [23]. These high-angular-momentum intermediate states provide the overlap needed to make resonant Raman transitions to the edge states possible with reasonable efficiency, as the edge states are spectrally isolated. Future theoretical studies are required for a quantitative estimate of the transfer probabilities and for determining the optimal parameters of the lasers. To image the edge states, one can use a direct *in situ* imaging techniques [24,25]. The method developed by the Greiner group has been recently deployed with a two-dimensional optical lattice trap and has produced single-site images of hundreds of atoms confined in a planar array.

IV. CONCLUSIONS

We propose the realization of topological quantum states with cold atoms in an optical lattice. A combination of a hexagonal optical lattice potential and a periodic light-induced vector potential represents a cold-atom realization of the Haldane model. We show that such a system is characterized by chiral edge modes, which are the signature of a topological quantum state. Observing these edge states is an

effective way of “seeing” a topological phase. We establish that the realization of a sharp boundary and the minimization of any smoothly varying component of the confining potential, e.g., of the harmonic confining potential, are necessary conditions for realizing a topological insulator with optical lattices. Controlling the confining potential opens the possibility of testing the stability of the chiral edge modes against weak disorder and interactions and, together with the control of the vector potential, offers a knob for tuning the system from a topological insulator state to a standard insulator or a metallic phase. While these general conclusions hold for any realization of a topological quantum state with cold atoms,

we find that the implementation of the Haldane model suffers from low-temperature limitations due to the chiral contributions to the Hamiltonian coming from second-neighbor hoppings, which are relatively small. The best way to overcome this limitation is by realizing the topological states in systems with nearest-neighbor anomalous hopping.

ACKNOWLEDGMENTS

This work is supported by NSF through JQI-PFC, DARPA, and USARO.

-
- [1] W. Kohn, Phys. Rev. **133**, A171 (1964).
 [2] X. G. Wen, Phys. Rev. B **44**, 2664 (1991).
 [3] D. J. Thouless, M. Kohmoto, M. P. Nightingale, and M. den Nijs, Phys. Rev. Lett. **49**, 405 (1982).
 [4] F. D. M. Haldane, Phys. Rev. Lett. **61**, 2015 (1988).
 [5] C. L. Kane and E. J. Mele, Phys. Rev. Lett. **95**, 226801 (2005).
 [6] L. Fu, C. L. Kane, and E. J. Mele, Phys. Rev. Lett. **98**, 106803 (2007); L. Fu and C. L. Kane, Phys. Rev. B **76**, 045302 (2007).
 [7] M. König, S. Wiedmann, C. Brune, A. Roth, H. Buhmann, L. W. Molenkamp, X.-L. Qi, and S.-C. Zhang, Science **318**, 766 (2007).
 [8] D. Hsieh, D. Qian, L. Wray, Y. Xia, Y. S. Hor, R. J. Cava, and M. Z. Hasan, Nature (London) **452**, 970 (2008).
 [9] V. W. Scarola and S. Das Sarma, Phys. Rev. Lett. **98**, 210403 (2007).
 [10] L. B. Shao, S.-L. Zhu, L. Sheng, D. Y. Xing, and Z. D. Wang, Phys. Rev. Lett. **101**, 246810 (2008).
 [11] R. Dum and M. Olshanii, Phys. Rev. Lett. **76**, 1788 (1996).
 [12] S. K. Dutta, B. K. Teo, and G. Raithel, Phys. Rev. Lett. **83**, 1934 (1999).
 [13] D. Jaksch and P. Zoller, New J. Phys. **5**, 56 (2003).
 [14] G. Juzeliunas and P. Ohberg, Phys. Rev. Lett. **93**, 033602 (2004); J. Ruseckas, G. Juzeliunas, P. Ohberg, and M. Fleischhauer, *ibid.* **95**, 010404 (2005).
 [15] K. Osterloh, M. Baig, L. Santos, P. Zoller, and M. Lewenstein, Phys. Rev. Lett. **95**, 010403 (2005).
 [16] A. Sorensen, E. Demler, and M. Lukin, Phys. Rev. Lett. **94**, 086803 (2005).
 [17] S. L. Zhu, H. Fu, C. J. Wu, S. C. Zhang, and L. M. Duan, Phys. Rev. Lett. **97**, 240401 (2006).
 [18] I. I. Satija, D. C. Dakin, and C. W. Clark, Phys. Rev. Lett. **97**, 216401 (2006).
 [19] T. D. Stanescu, C. Zhang, and V. M. Galitski, Phys. Rev. Lett. **99**, 110403 (2007).
 [20] Y.-J. Lin, R. L. Compton, A. R. Perry, W. D. Phillips, J. V. Porto, and I. B. Spielman, Phys. Rev. Lett. **102**, 130401 (2009).
 [21] T. D. Stanescu and V. Galitski, Phys. Rev. B **74**, 205331 (2006).
 [22] R. O. Umucalilar, H. Zhai, and M. O. Oktel, Phys. Rev. Lett. **100**, 070402 (2008).
 [23] M. F. Andersen, C. Ryu, P. Clade, V. Natarajan, A. Vaziri, K. Helmerson, and W. D. Phillips, Phys. Rev. Lett. **97**, 170406 (2006).
 [24] K. D. Nelson, X. Li, and D. S. Weiss, Nat. Phys. **3**, 556 (2007).
 [25] J. Gillen, W. Bakr, A. Peng, P. Unterwaditzer, S. Foelling, and M. Greiner, e-print arXiv:0812.3630; J. I. Gillen *et al.*, APS March Meeting, 2009 (unpublished).